ACS APPLIED MATERIALS & INTERFACES

Research Article

www.acsami.org

Multi-Stimulus-Responsive Shape-Memory Polymer Nanocomposite Network Cross-Linked by Cellulose Nanocrystals

Ye Liu, Ying Li, Guang Yang, Xiaotong Zheng, and Shaobing Zhou*

Key Laboratory of Advanced Technologies of Materials, Ministry of Education, School of Materials Science and Engineering, Southwest Jiaotong University, Chengdu, Sichuan 610031, P. R. China

ABSTRACT: In this study, we developed a thermoresponsive and water-responsive shape-memory polymer nanocomposite network by chemically cross-linking cellulose nanocrystals (CNCs) with polycaprolactone (PCL) and polyethylene glycol (PEG). The nanocomposite network was fully characterized, including the microstructure, cross-link density, water contact angle, water uptake, crystallinity, thermal properties, and static and dynamic mechanical properties. We found that the PEG[60]−PCL[40]−CNC[10] nanocomposite exhibited excellent thermo-induced and water-induced shape-memory effects in water at 37 °C (close to body temperature), and the introduction of CNC clearly improved the mechanical properties of the mixture of both PEG and PCL polymers with low molecular weights. In addition, Alamar blue assays based on osteoblasts indicated that the nanocomposites possessed good cytocompatibility. Therefore, this thermoresponsive and water-responsive shape-memory nanocomposite could be potentially developed into a new smart biomaterial.

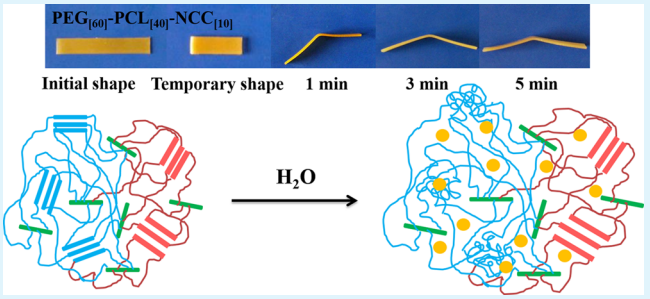

KEYWORDS: *shape memory, water-responsive, thermoresponsive, nanocomposite, cellulose nanocrystals*

INTRODUCTION

Shape-memory polymers (SMPs) have the ability to recover their original shape from a temporary shape[1] when they are exposed to an appropriate stimulus such as heat,[2−4] light,[5,6] electric field,[7−9] magnetic field,[10,11] or moisture.[12−14] In recent years, SMPs have gained an increasing amount of attention for their medical applications, such as smart sutures,[15] vascular stents,[16] esophageal stents,[17] and tissue engineering scaffolds,[18] and in drug delivery.[19,20] However, a major drawback of SMPs is their low tensile strength and stiffness in contrast with metals and ceramics, which limit their applications.[21] One of the ways to overcome this drawback is to prepare composites by introducing inorganic nanofillers into polymers such as SiO_2,[22] POSS,[23] and carbon nanotubes.[24] However, the improvement is limited because of the reinforcement with particles or short fibers.[25]

Currently, cellulose nanocrystals (CNCs) have been developed to be an ideal candidate for improving the mechanical properties of a targeted host material because of the nanoscale dimensions and extremely attractive mechanical properties of CNCs.[26] Furthermore, CNCs are the most abundant biopolymers and offer many advantages, such as low cost, low density, availability, renewability, biodegradability, and unsurpassed quintessential physical and chemical properties.[27,28] CNCs have attracted a great deal of interest and have been utilized as a nanofiller for polymer matrices in the field of nanocomposites.[29−33] However, to the best of our knowledge, most of these nanocomposites were obtained by physical incorporation of CNCs into the polymeric matrix. Consequently, the interaction between the nanofillers and the polymer molecular chains was not strong, subsequently leading to an inapparent increase in or even failure to improve the mechanical properties of the polymer. In particular, in most cases, the reported molecular weights of the polymer matrices are sufficiently high to meet the property requirements. Low-molecular weight polymers are seldom employed as the matrix of polymer composites because of their poor mechanical strength. Additionally, for shape-memory polymer composites, the introduction of nanoparticles into the polymer matrix by physical blending can affect the shape-memory performance and broaden the transition temperature.[34] Water-induced shape-memory polymer composites have received increasing amounts of attention in recent years because this stimulus is mild and friendly.[32,35] Therefore, the water-induced shape-memory composites developed in this study are especially attractive for potential biomedical applications, such as self-tightening sutures and self-retractable and removable stents.

In this study, a thermoresponsive and water-responsive shape-memory polymer nanocomposite network was synthesized by chemically cross-linking cellulose nanocrystals with polycaprolactone (PCL) and polyethylene glycol (PEG). Both PCL and PEG have been widely applied as biomaterials in medicine because of their good biocompatibility. The end hydroxyl groups of both PCL and PEG were first functionalized with 4,4-diphenylmethane diisocyanate (MDI), and this step was

Received: November 19, 2014
Accepted: February 3, 2015
Published: February 3, 2015

DOI: 10.1021/am5081056
ACS Appl. Mater. Interfaces 2015, 7, 4118−4126

followed by chemical cross-linking with the hydroxyl groups of CNCs. Both the PCL and PEG molecular weights (M_w) were low (4000 Da), and their mechanical strengths were very poor. However, after the chemical cross-linking with CNCs, the nanocomposite network displayed high tensile strength and stain-to-failure. This strategy could provide a potential platform for enhancing the mechanical strength of low-molecular weight polymers. Furthermore, the nanocomposite network exhibited thermoresponsive and water-responsive shape-memory functions. The advantages of this nanocomposite, including good hydrophilicity from the CNC and PEG components, biocompatibility, and controllable biodegradability, make it an attractive candidate for potential applications as biomaterials and environmentally friendly materials.

MATERIALS AND METHODS

Materials. PCL [number-average molecular weight (M_n) = 4 kDa; PDI = 1.65] was synthesized by ring-opening polymerization of ε-CL, as previously described.[36] Stannous octoate and ε-CL were purchased from Aldrich. PEG [weight-average molecular weight (M_w) = 4 kDa; PDI = 1.26] was purchased from Sigma. CNCs were prepared from microcrystalline cellulose (MCC) (Chengdu Reagent Factory) by hydrolysis treatment (64 wt % sulfuric acid in water for 1.5 h at 44 °C), according to a previously published method.[37] The average size and the size dispersity of CNC determined with a laser scattering particle size diffraction analyzer (Nano-ZS90, MALVERN) were 200 nm and 0.228, respectively. 4,4-Diphenylmethane diisocyanate (MDI) was purchased from Tokyo Chemical Industry Co. Ltd. and used without further treatment. All other chemicals and solvents were of reagent grade or better and purchased from Kelong chemical reagent factory (Chengdu, China).

Preparation of PEG−PCL−CNC Nanocomposites. Cellulose nanocrystal acetone gels were first prepared from aqueous dispersions using a solvent-exchange sol−gel process with a reported protocol.[38] Subsequently, the cellulose nanocrystal acetone gels, which contained 2 g of CNC, were dissolved in 50 mL of *N*-dimethylformamide (DMF), and a stable solution was obtained through a 10 min ultrasonic treatment. Later, the solution was dried over activated 4 Å molecular sieves for 7 days. The molecular sieves were changed once or twice daily. Finally, a stable solution in DMF was achieved with a solid content of 20 mg/mL. As a representative example, we describe the detailed procedure for preparing the PEG[60]−PCL[40]−CNC[10] nanocomposite. PEG (1.2 g, 0.3 mmol) and PCL (0.8 g, 0.2 mmol) were added to a 100 mL three-neck round flask, and this device was placed in an oil bath at 90 °C for 2 h under vacuum to remove the moisture. Subsequently, MDI (0.25 g, 1 mmol) was quickly added to this three-neck round flask, which was connected to a backflow device and Ar gas protection device and equipped with a magnetic stirrer. The reaction was conducted at 80 °C for 3 h. Then, 12.5 mL of the stable cellulose nanocrystal solution in DMF and stannous octoate were added to the system. After the reaction mixture had been vigorously stirred for 1 h, the mixture was poured into a Teflon dish, which was kept at 85 °C for 24 h under a constant nitrogen flow. Finally, the obtained products were dried under vacuum for 24 h at 80 °C. Three different nanocompositions of the PEG−PCL−CNC nanocomposites were prepared (PEG[50]−PCL[50]−CNC[10], PEG[60]−PCL[40]−CNC[10], and PEG[70]−PCL[30]−CNC[10]), in which the numerical values after the PEG and PCL indicate the feed weight percent ratio of the PEG and PCL and the numerical values after the CNC indicate the weight percent of CNC in the nanocomposites.

Characterization. Fourier transform infrared spectroscopy (FT-IR) of all of the samples was conducted on a Nicolet 5700 IR spectrometer using the single-reflection attenuated total reflectance (ATR) system, and the number of scans was 64. XPS measurements were performed by ESCALAB Mark II X-ray photoelectron spectroscopy (XPS, VG Scientific) using monochromatic Mg Kα radiation from a Mg anode source. The high-resolution scans of core level spectra were set to a pass energy of 15 eV and recorded with an energy step of 0.05 eV. All of the obtained experimental data were deconvolved by Gaussian−Lorentzian mixture peak-fitting software. The gel fraction was evaluated as described in our previous report.[39] All of the preweighed specimens were immersed in dichloromethane for 24 h at room temperature. Then, the insoluble gel was separated by a high-speed centrifuge. Later, the gel was dried under vacuum until the mass remained unchanged. Consequently, the gel fraction was calculated according to the formula M_1/M_0, where M_0 is the weight of the specimen before immersion in dichloromethane and the M_1 is the weight of the dried insoluble gel. The fracture surfaces of the composites were investigated using an S-3500 scanning electron microscope. The samples were sputter-coated with gold prior to SEM observation. The accelerating voltage and magnification level were 10.0 kV and 10000×, respectively. Contact angle equipment (DSA 100, KRUSS) was used to measure the water contact angle by the sessile drop method at room temperature. All of the contact angle data were the averages of five measurements obtained at different locations on the sample surfaces. The water uptake of the samples was calculated by measuring the samples' weights before and after immersion in deionized water at 37 °C. The weight ratio of absorbed water was calculated by the formula $(M_1 - M_0)/M_0$, where M_1 refers to the weight of the sample after immersion in water at 37 °C and M_0 refers to the weight of the sample before immersion in water. Differential scanning calorimetry (DSC) measurements were performed on a TA DSC-Q100 under a continuous nitrogen purge. All of the samples were heated from −50 to 160 °C at a heating rate of 10 °C min^{-1}. Three heating cycles were conducted to measure all of the samples, and each sample was cooled to −50 °C. Samples immersed in water at 37 °C for 2 min were dried gently using tissue paper and characterized from 0 to 80 °C at a heating rate of 10 °C min^{-1}. X-ray diffractometry (XRD) (Philips, X'Pert PRO) was used to determine the crystallization property of the composites. After being immersed in water at 37 °C for 2 min, the samples were gently dried using tissue paper. The samples were scanned from 2θ values of 5° to 60°. The tensile properties of the samples at room temperature were measured on an Instron 5567 (Instron Co.) instrument. The extension rate was 1 mm min^{-1}. After being immersed in water at 37 °C for 30 min, the samples were gently dried using tissue paper. The measurements were taken at 37 °C, with an extension rate of 1 mm min^{-1}. The dynamic mechanical properties of the composites were measured by a TA DMA-Q 800 instrument using the tensile resonant mode from 0 to 80 °C at a heating rate of 3 °C min^{-1} and a constant frequency of 1 Hz. The test specimen dimensions were 30 mm × 4 mm × 0.15 mm (length × width × thickness). The thermoresponsive shape-memory effect was investigated as follows. First, the rectangular strip sample was folded by deformation at 60 °C, and the temperature was reduced to −10 °C under constant stress to fix the temporary shape. Then, the sample with a deformed shape was placed in an oven at 60 °C. The shape recovery process was recorded using a video camera. The shape-memory fixity ratio (R_f) and recovery ratio (R_r) were investigated using a rectangular strip sample and conducted on a DMA (TA DMA-Q 800) instrument using the controlled force mode. First, the specimen was strained at a stress rate of 0.5 MPa/min to 1.5 MPa at 60 °C; a temporary shape was obtained, and the strain was marked as ε_m. Second, the temperature was decreased to −10 °C under constant stress; the stress was released, and the strain was marked as ε_1. Finally, the fixed temporary shape was heated at 60 °C for 15 min, and the final strain was marked as ε_2. R_f and R_r were calculated according to the following equations:

$$R_f = \frac{\varepsilon_1}{\varepsilon_m} \times 100\% \quad (1)$$

$$R_r = \frac{\varepsilon_m - \varepsilon_2}{\varepsilon_m} \times 100\% \quad (2)$$

The water-responsive shape-memory effect was investigated as described in our previous report.[40] First, the rectangular strip samples were folded by deformation at 60 °C, and the temperature was decreased to −10 °C under constant stress to fix the temporary shape. Second, the fixed sample was immersed in water at 37 °C. Then, images of the shape recovery were recorded using a video camera. The recovery ratio was defined as $[(\theta - \theta_0)/(180 - \theta_0)] \times 100\%$, where θ refers to the angle of

DOI: 10.1021/am5081056
ACS Appl. Mater. Interfaces 2015, 7, 4118−4126

Scheme 1. Synthetic Route of the PEG−PCL−CNC Nanocomposite Network

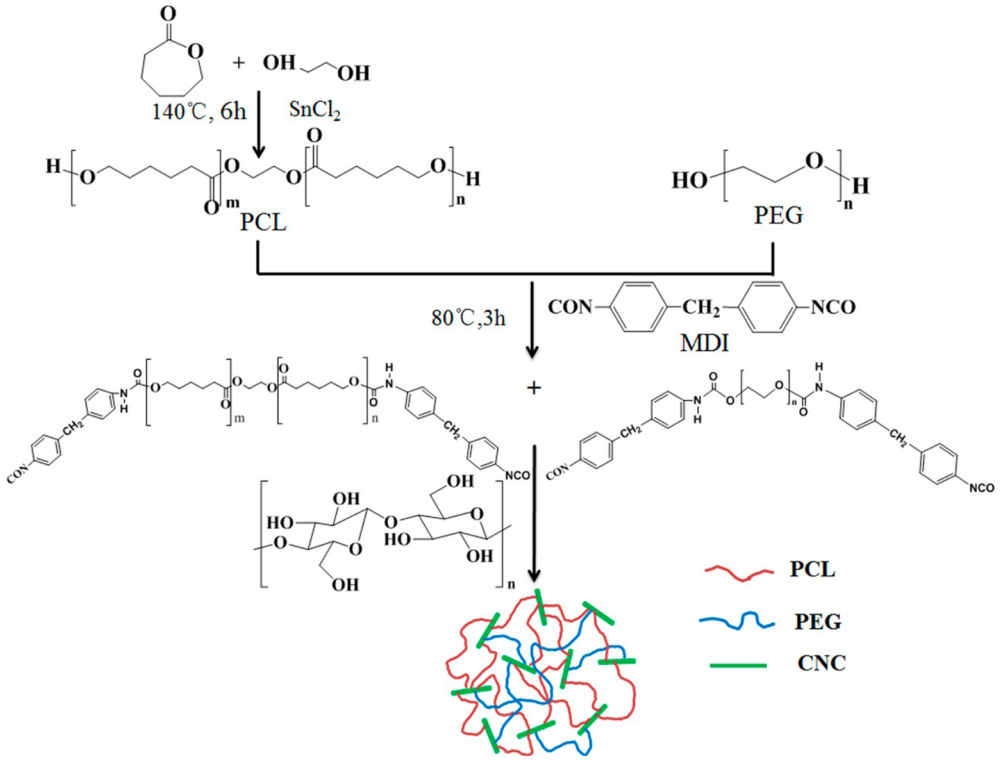

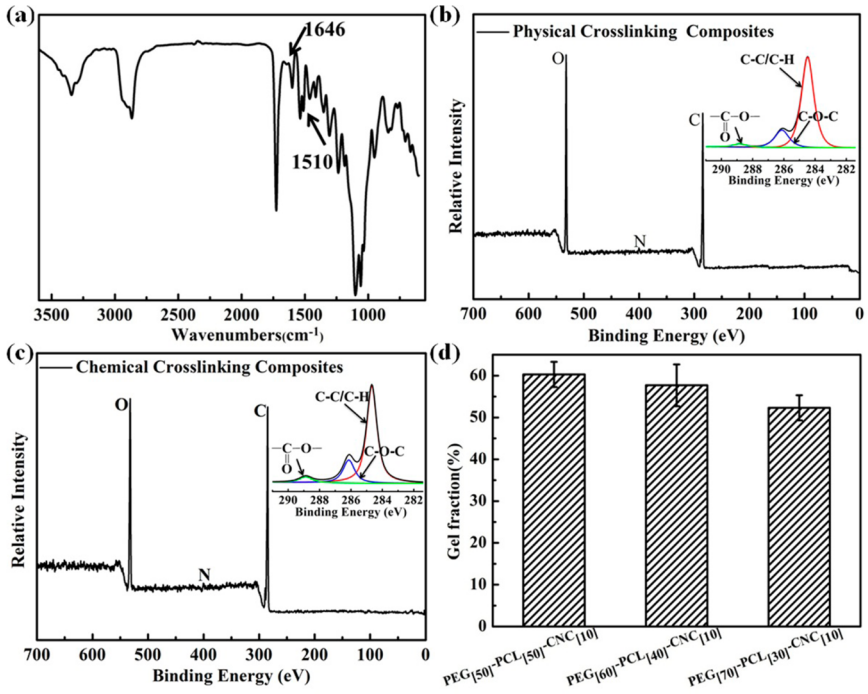

Figure 1. (a) FTIR spectrum of the PEG[60]−PCL[40]−CNC[10] nanocomposite. (b) XPS wide scans of the PEG[60]−PCL[40]−CNC[10] physically cross-linked nanocomposite. (c) XPS wide scans of the PEG[60]−PCL[40]−CNC[10] chemically cross-linked nanocomposite (insets show high-resolution carbon spectra). (d) Gel fractions of the PEG[60]−PCL[40]−CNC[10] nanocomposite.

the folded specimen at a given time at 37 °C and θ_0 indicates the angle at 0 min. The results represent the averages of at least three specimens.

Cytotoxicity Analysis. The cytotoxicity was evaluated by an Alamar blue assay as described in our previous report.[41] Briefly, all of the small round flake samples with an average diameter of approximately 15 mm were sterilized by being immersed in ethanol (75%) for 2 h and remained in sterilized PBS overnight. Subsequently, the samples were used for osteoblast culturing in vitro. The cell viability ratio (R) for each sample was calculated using the equation R = (cell viability in the experiment)/(cell viability in the negative control). The cell morphology was investigated by fluorescence microscopy (DMIL, Leica). The live osteoblast cells grown on the samples for 3 and 7 days were stained with a 5% (v/v) calcein solution (diluted in PBS) for

DOI: 10.1021/am5081056
ACS Appl. Mater. Interfaces 2015, 7, 4118−4126

approximately 5 min and immediately observed by fluorescence microscopy.

RESULTS AND DISCUSSION

Characterization of the PEG−PCL−CNC Nanocomposites. The synthetic route of the PEG−PCL−CNC nanocomposite network is shown in Scheme 1. Urethane linkages formed between CNC and the molecular chains of the isocyanate-terminated PEG and PCL. By varying the weight ratio of PCL and PEG, we could successfully prepare PEG−PCL−CNC nanocomposites with different compositions.

Fourier transform infrared spectroscopy (FT-IR) was employed to confirm the chemical structure of the nanocomposite network. From the spectra of the PEG[60]−PCL[40]−CNC[10] nanocomposites in Figure 1a, we observed two clear peaks at 1646 and 1510 cm^{-1} that corresponded to the absorption of carbonyl groups (C═O) and N−H bending deformation combined with C−N asymmetric stretching, respectively.[31] Furthermore, a clear peak at 2270 cm^{-1} was observed, which corresponds to the absorption of unreacted isocyanate,[42] indicating that the hydroxyl group of CNC successfully reacted with MDI.

To evaluate whether PEG and PCL were cross-linked chemically or physically with CNC fillers, X-ray photoelectron spectroscopy (XPS) was used to determine the main elements and the carbon-based bonds of this nanocomposite network. As shown in panels b and c of Figure 1, the low-resolution spectra of all of the nanocomposites showed that carbon and oxygen atoms were the main components, whereas less nitrogen was also present. In the high-resolution carbon spectra, the carbon signal could be resolved into several component peaks, which reflected the local environments of the carbon atoms (C−C and C−H or C−O−C or O−C═O). We also found that the relative amount of O−C═O in the PEG[60]−PCL[40]−CNC[10] chemically cross-linked nanocomposite was greater than that in the PEG[60]−PCL[40]−CNC[10] physically cross-linked nanocomposite, although the feed ratio was the same. These results also indicated that the hydroxyl groups of CNC successfully reacted with MDI.

Figure 1d displays the gel fractions of all of the nanocomposites. It can be observed that the gel fraction of the PEG[50]−PCL[50]−CNC[10] nanocomposite was the largest in all of the nanocomposites. In addition, the gel fraction of the composites decreased as the PEG component increased. However, the gel fractions of all of the nanocomposites were approximately 60%. The results also indicate that the chemical cross-linking reaction occurred, which was mainly ascribed to the fact that the hydroxyl groups of CNC reacted with the diisocyanate. Because CNC has a large number of hydroxyl groups, it can be used as a cross-linker to cross-link the molecular chains of PCL and PEG whose ends were blocked by diisocyanate.

Morphology of the PEG−PCL−CNC Nanocomposites. The fracture surfaces of samples, including the PEG[60]−PCL[40]−CNC[10] and PEG[70]−PCL[30]−CNC[10] nanocomposites, were observed by scanning electron microscopy (SEM). From Figure 2, white dots could be clearly identified in the matrix of the nanocomposites, which corresponded to the CNC in the perpendicular plane of the nanocomposite.[43,44] The inset displays the greater magnification of the fractured surface of the nanocomposite, and it could be clearly observed that the CNC fillers inserted into the PCL−PEG matrix. In addition, as shown in Figure 2, these CNC fillers were well dispersed in the PCL−PEG matrix, implying that a good compatibility between the nanofillers and polymer matrix was achieved, which may be ascribed to the covalent bonding between CNC and the molecular chains of the PEG and PCL.[45]

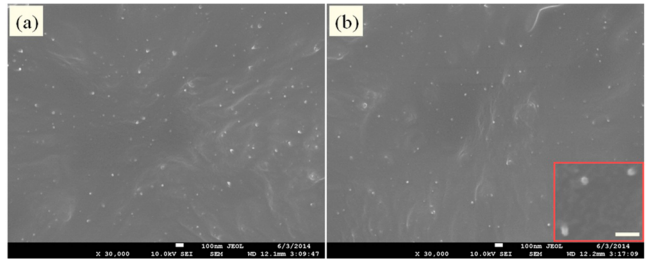

Figure 2. Cross-sectional SEM image showing the fracture surface of the PEG−PCL−CNC nanocomposites: (a) PEG[60]−PCL[40]−CNC[10] and (b) PEG[70]−PCL[30]−CNC[10]. The inset is magnified (scale bar of 100 nm).

Thermal and Crystalline Properties. Figure 3a shows the DSC results of the nanocomposites. The glass transition temperatures of all of the nanocomposites were approximately 42 °C, which is close to body temperature. The transition temperature of the nanocomposite was significantly lower than those of the pure PEG and PCL, which could be attributed to decreased crystallinity of the PEG and PCL after cross-linking by the CNC. We calculated the crystallinity from DSC, which was determined using the heat of fusion of 100% crystalline PCL and PEG. The crystallinity of the PEG[50]−PCL[50]−CNC[10] nanocomposite was 21.2%, the crystallinity of the PEG[60]−PCL[40]−CNC[10] nanocomposite 29.1%, and the crystallinity of the PEG[70]−PCL[30]−CNC[10] nanocomposite 39.8%. Furthermore, the PEG[50]−PCL[50]−CNC[10] nanocomposite had two melting points, which may be because the PEG and PCL possessed the same weight ratio, and the two components competitively crystallized in the nanocomposite. However, when the PEG component was dominant in the nanocomposites, the PEG component crystallized first, which tended to suppress the growth of PCL crystallites.[46] The microphase morphologies of the nanocomposites were further characterized using X-ray diffractometry (XRD), and there were three clear diffraction peaks (Figure 3b). The crystalline peaks at $2\theta = 19.3°$ were attributed to the 120 planes of the PEG monoclinic unit cell; the crystalline peaks located at $2\theta = 21.5°$ were indexed as the (110) planes of the PCL crystallites, and the crystalline peaks located at $2\theta = 23.5°$ were the superposition of the (200) planes of the PCL crystallites and diverse PEG reflections.[47,48] Furthermore, as the PEG component increased, the intensity of the diffraction peaks of the PCL crystallites decreased, whereas the diffraction peaks of the PEG crystallites became stronger. This result was mainly ascribed to the fact that the PEG component was dominant in the nanocomposites; therefore, the PEG component crystallized first and suppressed the growth of the PCL crystallites. These results were in accordance with the DSC results.

Mechanical Properties. Figure 4a shows typical stress−strain curves for the nanocomposites. As the PEG component increased, the tensile stress increased, whereas the elongation to break clearly decreased, which may be attributed to the high crystallinity of the nanocomposites with a high PEG component. It can also be observed that the PEG[60]−PCL[40]−CNC[10] nanocomposite had better mechanical properties. The tensile stress was 6.28 MPa, and the elongation to break was 161.28%. This result demonstrated that the introduction of 10% CNC into the PEG and PCL matrix could improve the mechanical

DOI: 10.1021/am5081056
ACS Appl. Mater. Interfaces 2015, 7, 4118−4126

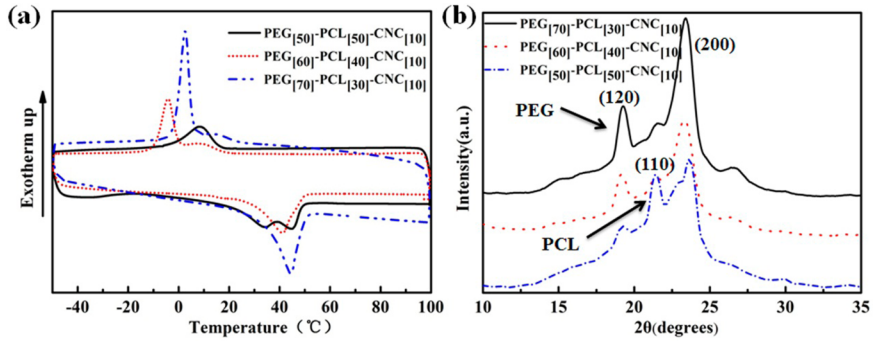

Figure 3. DSC and XRD results of the PEG−PCL−CNC nanocomposites: (a) DSC and (b) XRD.

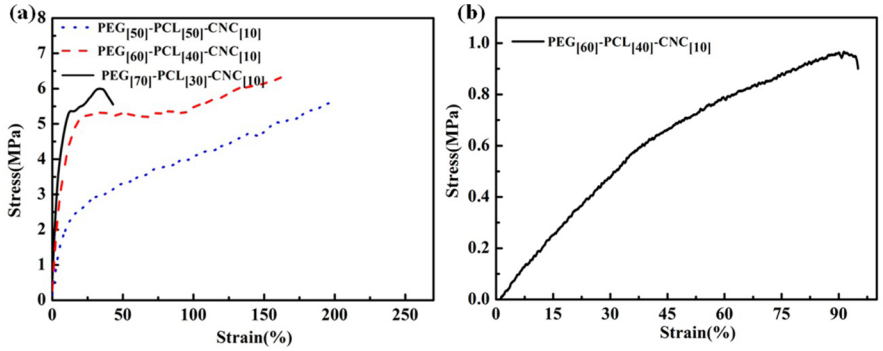

Figure 4. Typical stress−strain curves of the PEG−PCL−CNC nanocomposites: (a) in the dry state and (b) in the wet state.

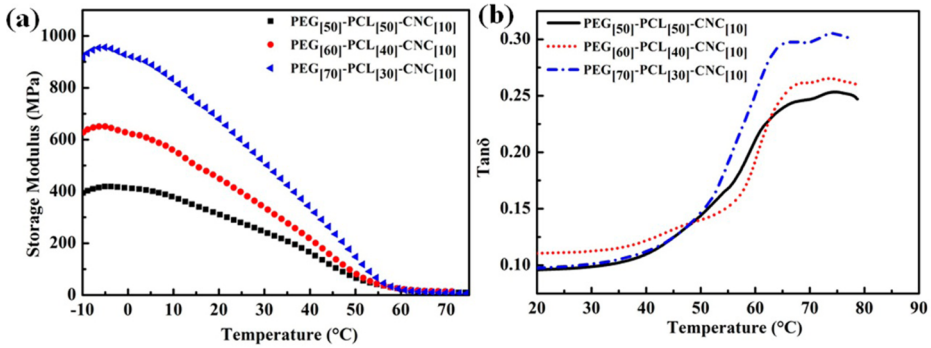

Figure 5. DMA analysis of the PEG−PCL−CNC nanocomposites: (a) storage modulus and (b) tan δ curves.

properties. However, for the nanocomposite composed of low molecular weights of both PEG and PCL physically mixed with CNC fillers, its mechanical properties were very poor. Therefore, the chemical cross-linking of CNC with PEG and PCL plays a crucial role in achieving a high mechanical strength for low-molecular weight polymers.

Figure 4b shows a typical stress−strain curve of the PEG[60]−PCL[40]−CNC[10] nanocomposite after immersion in water at 37 °C for 30 min. In comparison with the mechanical properties of the PEG[60]−PCL[40]−CNC[10] nanocomposite in the dry state, we found that both the tensile stress and elongation to break decreased in the wet state. This result could be ascribed to the fact that the hydrophilic PEG component was dissolved after the water molecules penetrated into the nanocomposite.

Dynamic Mechanical Properties. Figure 5 shows the storage modulus and tan δ curves of the nanocomposites as a function of temperature. As the PEG component increased, the storage modulus of the nanocomposites significantly increased. For example, the storage modulus of the PEG[60]−PCL[40]−CNC[10] nanocomposite was 630 MPa at 0 °C in the glassy state, whereas the storage modulus decreased to approximately 0 MPa at 70 °C in the rubbery state. A decrease of up to 2 orders of magnitude occurred at temperatures ranging from 0 to 70 °C. Such a large difference in the storage modulus was proven to make an immense contribution to a good shape-memory effect. As the PEG component increased, a slight decrease in the tan δ value could be observed in Figure 5b, indicating that the mobility of the molecular chains also decreased.[49,50] The decrease in tan δ may better contribute to the shape-memory property.

Thermoresponsive Shape-Memory Properties. Figure 6a displays the thermoresponsive shape recovery behavior of the nanocomposites. The rectangular strip nanocomposites were folded by deformation at 60 °C, and the temperature was immediately decreased to −10 °C under constant stress to fix the temporary shape. Next, the deformed sample was placed in an oven at 60 °C. As shown in Figure 6a, the R_f of the PEG[50]−PCL[50]−CNC[10] nanocomposite and the R_r of the PEG[70]−PCL[30]−CNC[10] nanocomposite were lower

DOI: 10.1021/am5081056
ACS Appl. Mater. Interfaces 2015, 7, 4118−4126

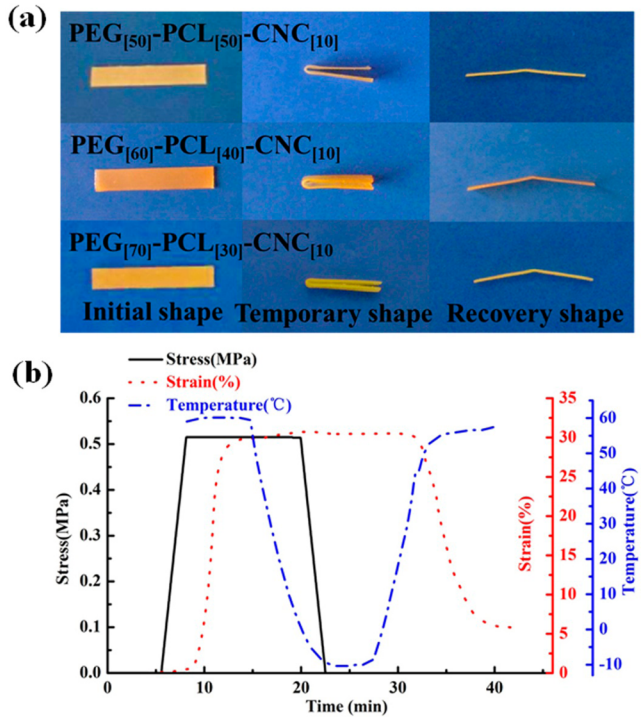

Figure 6. (a) Thermoresponsive shape-memory process of the PEG−PCL−CNC nanocomposites and (b) DMA curves of the PEG[60]−PCL[40]−CNC[10] nanocomposite.

than those of the other nanocomposites. These results were mainly ascribed to the fact that the PEG[50]−PCL[50]−CNC[10] nanocomposite had a lower crystallinity and the PEG[70]−PCL[30]−CNC[10] nanocomposite had a lower cross-linking degree, respectively. However, the PEG[60]−PCL[40]−CNC[10] nanocomposite possessed a better shape-memory property. R_f and R_r were approximately 100 and 90%, respectively.

The quantitative results of the shape-memory properties for the PEG[60]−PCL[40]−CNC[10] nanocomposite are shown in Figure 6b, in which the stress−strain−temperature curves were obtained in controlled force mode from DMA testing. The sample was elongated to a certain length at 60 °C, and then the temperature was decreased to −10 °C under constant stress to fix the temporary shape. Next, the fixed temporary shape was heated at 60 °C for 15 min. R_f and R_r were calculated according to eqs 1 and 2. R_f and R_r reached 100 and 85%, respectively. R_r was slightly decreased, which may be because the deformation in the cyclic tensile test was too large and the cross-linking degree of the PEG[60]−PCL[40]−CNC[10] nanocomposite was too low. Thus, in the cyclic tensile test, irreversible deformation occurred.

Water-Responsive Shape-Memory Properties. Through the analysis described above, we found that the PEG[60]−PCL[40]−CNC[10] nanocomposite had the best thermoresponsive shape recovery effect. Therefore, only the PEG[60]−PCL[40]−CNC[10] nanocomposite was employed to investigate the water-responsive shape recovery behavior. The rectangular strip nanocomposite was folded by deformation at 60 °C, and the temporary shape was fixed at −10 °C under constant stress. Next, the sample with a deformed shape was immersed in water at 37 °C. As shown in Figure 7, the PEG[60]−PCL[40]−CNC[10] nanocomposite reached the maximal shape-memory recovery ratio, and the R_r value was 86%. It can also be observed that the sample had a certain degree of swelling.

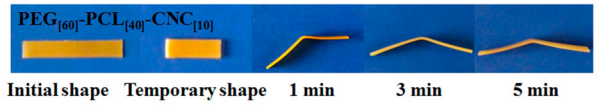

Figure 7. Water-responsive shape-memory process of the PEG−PCL−CNC nanocomposites in water at 37 °C.

These results were mainly ascribed to the fact that the PEG[50]−PCL[50]−CNC[10] nanocomposite absorbed a certain amount of water.

Mechanism of the Water-Responsive Shape-Memory Effect. Figure 8a shows the adsorbed water fraction in weight percent of the PEG[60]−PCL[40]−CNC[10] nanocomposite versus immersion time at 37 °C, and the inset shows the water contact angle analysis. It can be observed that the PEG[60]−PCL[40]−CNC[10] nanocomposite held a contact angle of 82.6°, indicating that it was hydrophilic. The hydrophilic surface could be useful for biomaterials to favor cell attachment.[51] In addition, the PEG[60]−PCL[40]−CNC[10] nanocomposite absorbed a 41% weight percentage of water after immersion in water for 2 min, and the maximal absorbed water content reached 100% after immersion for 20 min.

Figure 8b displays the DSC curves of the PEG[60]−PCL[40]−CNC[10] nanocomposite before and after immersion in water at 37 °C for 2 min. The transition temperature decreased to <40 °C, and a wide transition temperature occurred after the absorption of a certain amount of water. These results were mainly ascribed to the fact that the H_2O molecules in the nanocomposite acted as a plasticizer and improved the mobility of the polymer molecular chains, which was consistent with previous reports.[52,53]

Figure 8c displays the XRD results of the PEG[60]−PCL[40]−CNC[10] nanocomposite before and after immersion in water at 37 °C for 2 min. The diffraction peaks of the PEG crystallites disappeared because of the dissolution of the hydrophilic PEG component,[54] whereas the diffraction peaks of the PCL crystallites remained because of the strong hydrophobicity after the absorption of a certain amount of water.

Therefore, the proposed water-responsive shape-memory mechanism for the PEG[60]−PCL[40]−CNC[10] nanocomposite is shown in Figure 8d. On one hand, in the wet state, some water diffused into the PEG[60]−PCL[40]−CNC[10] nanocomposite matrix and in turn acted as a plasticizer, which led to a decrease in the transition temperature of the composites and broadened the transition temperature until shape recovery occurred. On the other hand, the PEG component dissolved upon immersion in water, resulting in the disappearance of the melting point and subsequent recovery of the permanent shape.[55,56]

Cytotoxicity Analysis. Each component, among PCL, PEG, and CNC, has good biocompatibility, as reported in the literature.[27,28,36] Additionally, in our previous report, we investigated the effect of the amount ratio of cellulose crystals and polylactide on the cytocompatibility, and the result showed that the amount ratio of the composites did not influence the biocompatibility.[40] Therefore, here we only evaluated the biocompatibility of one amount ratio. The *in vitro* cytotoxicity of the PEG[60]−PCL[40]−CNC[10] nanocomposite was assessed by measuring the viability of osteoblast cells. From Figure 9a, it can be observed that the cell viability remained greater than 88% after the cells had been cultured for both 3 and 7 days. This result indicated that the PEG[60]−PCL[40]−CNC[10] nanocomposite showed low cytotoxicity to normal

DOI: 10.1021/am5081056
ACS Appl. Mater. Interfaces 2015, 7, 4118−4126

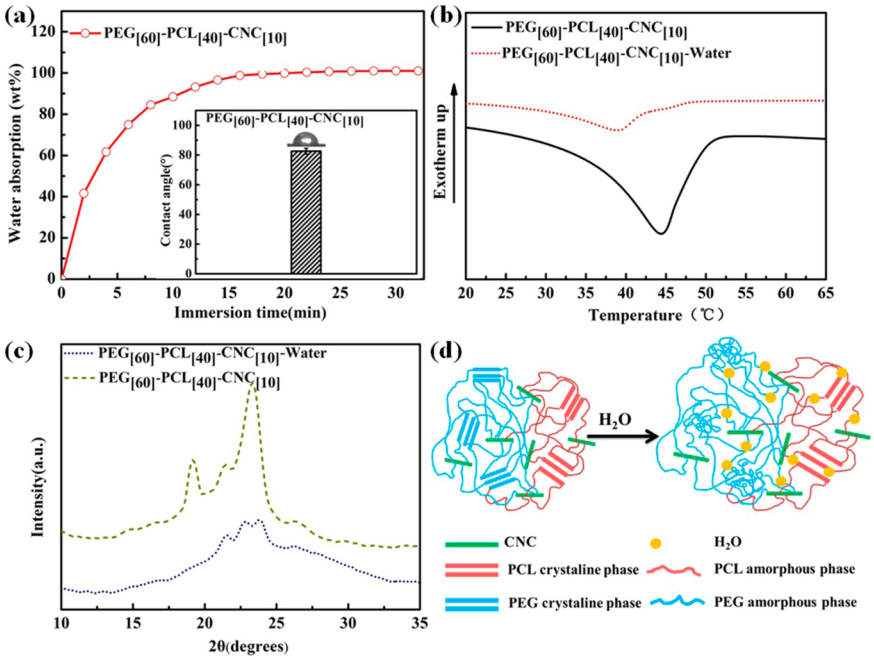

Figure 8. (a) Ratio of absorbed water to sample weight vs immersion time. The inset shows the water contact angle of the nanocomposite. (b) DSC results of the PEG−PCL−CNC nanocomposite before and after immersion in water at 37 °C for 2 min. (c) XRD results of the PEG−PCL−CNC nanocomposite before and after immersion in water at 37 °C for 2 min. (d) Water-responsive shape-memory mechanism of the PEG−PCL−CNC nanocomposite.

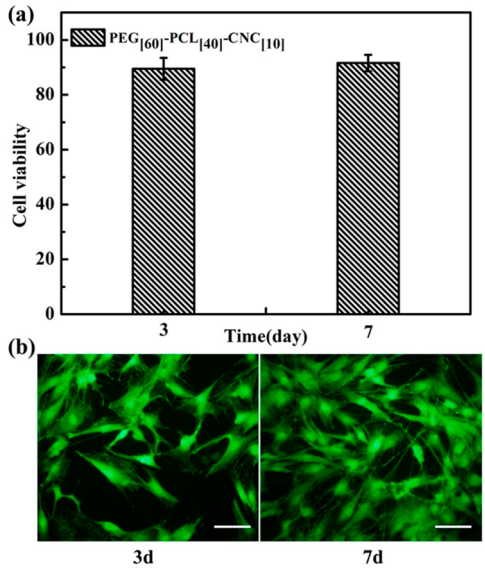

Figure 9. (a) Cytotoxicity of osteoblast cells cultured on the PEG−PCL−CNC nanocomposite. (b) Fluorescence microscope images of osteoblast cells cultured on the PEG−PCL−CNC nanocomposite for 3 and 7 days. Each scale bar represents 100 μm.

cells. Furthermore, the morphologies of the osteoblast cells cultured on the PEG[60]−PCL[40]−CNC[10] nanocomposite were observed by fluorescence microscopy after they had been stained with calcein. As shown in Figure 9b, it can be observed that the osteoblast cells established healthy cell morphologies. These results suggested that the PEG[60]−PCL[40]−CNC[10] nanocomposite held good cytocompatibility.

CONCLUSIONS

In summary, we successfully prepared one type of thermoresponsive and water-responsive shape-memory nanocomposite network with PCL and PEG as soft segments and CNC nanofillers as cross-linkers. The chemical cross-linking of 10% CNC with both PCL and PEG with low molecular weights could significantly improve the mechanical strength of the nanocomposite network. Simultaneously, the PEG[60]−PCL[40]−CNC[10] nanocomposite exhibited an excellent thermoresponsive and water-responsive shape-memory effect. Furthermore, good cytocompatibility was maintained upon the introduction of CNC into the biocompatible PCL and PEG polymer. Therefore, the multi-stimulus-responsive shape-memory polymer network could be potentially applied in the biomedical field, in applications such as self-tightening sutures and self-retractable smart stents.

AUTHOR INFORMATION

Corresponding Author

*Telephone: +86 28 87634068. Fax: +86 28 87634649. E-mail: shaobingzhou@swjtu.edu.cn.

Notes

The authors declare no competing financial interest.

ACKNOWLEDGMENTS

This work was partially supported by the National Basic Research Program of China (973 Program, 2012CB933600), the National Natural Science Foundation of China (51173150, 51203130, and 51373138), the National Key Project of Scientific and Technical Supporting Programs Funded by MSTC (2012BAI17B06), the Research Fund for the Doctoral Program of Higher Education of China (20120184110029), and the Construction Program for Innovative Research Team of University in Sichuan Province (14TD0050).

DOI: 10.1021/am5081056
ACS Appl. Mater. Interfaces 2015, 7, 4118−4126

REFERENCES

(1) Lendlein, A.; Kelch, S. Shape-Memory Polymers. *Angew. Chem., Int. Ed.* **2002**, *41*, 2034−2057.
(2) Ratna, D.; Karger-Kocsis, J. Recent Advances in Shape Memory Polymers and Composites: A Review. *J. Mater. Sci.* **2008**, *43*, 254−269.
(3) Liu, C.; Qin, H.; Mather, P. T. Review of Progress in Shape-Memory Polymers. *J. Mater. Chem.* **2007**, *17*, 1543−1558.
(4) Zheng, X. T.; Zhou, S. B.; Li, X. H.; Weng, J. Shape Memory Properties of Poly(D,L-Lactide)/Hydroxyapatite Composites. *Biomaterials* **2006**, *27*, 4288−4295.
(5) Lendlein, A.; Jiang, H.; Jünger, O.; Langer, R. Light-Induced Shape-Memory Polymers. *Nature* **2005**, *434*, 879−882.
(6) Jiang, H.; Kelch, S.; Lendlein, A. Polymers Move in Response to Light. *Adv. Mater. (Weinheim, Ger.)* **2006**, *18*, 1471−1475.
(7) Liu, Y.; Lv, H.; Lan, X.; Leng, J.; Du, S. Review of Electro-Active Shape-Memory Polymer Composite. *Compos. Sci. Technol.* **2009**, *69*, 2064−2068.
(8) Luo, X.; Mather, P. T. Conductive Shape Memory Nanocomposites for High Speed Electrical Actuation. *Soft Matter* **2010**, *6*, 2146−2149.
(9) Xiao, Y.; Zhou, S. B.; Wang, L.; Gong, T. Electro-Active Shape Memory Properties of Poly(ε-Caprolactone)/Functionalized Multiwalled Carbon Nanotube Nanocomposite. *ACS Appl. Mater. Interfaces* **2010**, *2*, 3506−3514.
(10) Mohr, R.; Kratz, K.; Weigel, T.; Lucka-Gabor, M.; Moneke, M.; Lendlein, A. Initiation of Shape-Memory Effect by Inductive Heating of Magnetic Nanoparticles in Thermoplastic Polymers. *Proc. Natl. Acad. Sci. U.S.A.* **2006**, *103*, 3540−3545.
(11) Zheng, X. T.; Zhou, S. B.; Xiao, Y.; Yu, X. J.; Li, X. H.; Wu, P. Z. Shape Memory Effect of Poly(D,L-Lactide)/Fe_3O_4 Nanocomposites by Inductive Heating of Magnetite Particles. *Colloids Surf., B* **2009**, *71*, 67−72.
(12) Yang, B.; Huang, W.; Li, C.; Lee, C.; Li, L. On The Effects of Moisture in a Polyurethane Shape Memory Polymer. *Smart Mater. Struct.* **2004**, *13*, 191−195.
(13) Chen, S.; Hu, J.; Yuen, C.-w.; Chan, L. Novel Moisture-Sensitive Shape Memory Polyurethanes Containing Pyridine Moieties. *Polymer* **2009**, *50*, 4424−4428.
(14) Chen, S.; Hu, J.; Zhuo, H. Study on the Moisture Absorption of Pyridine Containing Polyurethane for Moisture-Responsive Shape Memory Effects. *J. Mater. Sci.* **2011**, *46*, 6581−6588.
(15) Lendlein, A.; Langer, R. Biodegradable, Elastic Shape-Memory Polymers for Potential Biomedical Applications. *Science* **2002**, *296*, 1673−1676.
(16) Yakacki, C. M.; Shandas, R.; Lanning, C.; Rech, B.; Eckstein, A.; Gall, K. Unconstrained Recovery Characterization of Shape-Memory Polymer Networks for Cardiovascular Applications. *Biomaterials* **2007**, *28*, 2255−2263.
(17) Yu, X. J.; Wang, L.; Huang, M. T.; Gong, T.; Li, W. B.; Cao, Y. L.; Ji, D. J.; Wang, P.; Wang, J.; Zhou, S. B. A Shape Memory Stent of Poly(ε-Caprolactone-Co-DL-Lactide) Copolymer for Potential Treatment of Esophageal Stenosis. *J. Mater. Sci.: Mater. Med.* **2012**, *23*, 581−589.
(18) Liu, X.; Zhao, K.; Gong, T.; Song, J.; Bao, C. Y.; Luo, E.; Weng, J.; Zhou, S. B. Delivery of Growth Factors Using a Smart Porous Nanocomposite Scaffold to Repair a Mandibular Bone Defect. *Biomacromolecules* **2014**, *15*, 1019−1030.
(19) Wischke, C.; Neffe, A. T.; Steuer, S.; Lendlein, A. Evaluation of a Degradable Shape-Memory Polymer Network as Matrix for Controlled Drug Release. *J. Controlled Release* **2009**, *138*, 243−250.
(20) Gong, T.; Zhao, K.; Wang, W. X.; Chen, H. M.; Wang, L.; Zhou, S. B. Thermally Activated Reversible Shape Switch of Polymer Particles. *J. Mater. Chem. B* **2014**, *2*, 6855−6866.
(21) Auad, M. L.; Contos, V. S.; Nutt, S.; Aranguren, M. I.; Marcovich, N. E. Characterization of Nanocellulose-Reinforced Shape Memory Polyurethanes. *Polym. Int.* **2008**, *57*, 651−659.
(22) Zhang, Y.; Wang, Q.; Wang, C.; Wang, T. High-Strain Shape Memory Polymer Networks Crosslinked by SiO_2. *J. Mater. Chem.* **2011**, *21*, 9073−9078.
(23) Mya, K. Y.; Gose, H. B.; Pretsch, T.; Bothe, M.; He, C. Star-Shaped POSS-Polycaprolactone Polyurethanes and Their Shape Memory Performance. *J. Mater. Chem.* **2011**, *21*, 4827−4836.
(24) Sahoo, N. G.; Jung, Y. C.; Yoo, H. J.; Cho, J. W. Influence of Carbon Nanotubes and Polypyrrole on the Thermal, Mechanical and Electroactive Shape-Memory Properties of Polyurethane Nanocomposites. *Compos. Sci. Technol.* **2007**, *67*, 1920−1929.
(25) Leng, J.; Lan, X.; Liu, Y.; Du, S. Shape-Memory Polymers and Their Composites: Stimulus Methods and Applications. *Prog. Mater. Sci.* **2011**, *56*, 1077−1135.
(26) Habibi, Y.; Lucia, L. A.; Rojas, O. J. Cellulose Nanocrystals: Chemistry, Self-Assembly, and Applications. *Chem. Rev.* **2010**, *110*, 3479−3500.
(27) De Souza Lima, M. M.; Borsali, R. Rodlike Cellulose Microcrystals: Structure, Properties, and Applications. *Macromol. Rapid Commun.* **2004**, *25*, 771−787.
(28) Azizi Samir, M. A. S.; Alloin, F.; Dufresne, A. Review of Recent Research into Cellulosic Whiskers, their Properties and Their Application in Nanocomposite Field. *Biomacromolecules* **2005**, *6*, 612−626.
(29) Habibi, Y.; Goffin, A.-L.; Schiltz, N.; Duquesne, E.; Dubois, P.; Dufresne, A. Bionanocomposites Based on Poly(ε-Caprolactone)-Grafted Cellulose Nanocrystals by Ring-Opening Polymerization. *J. Mater. Chem.* **2008**, *18*, 5002−5010.
(30) Jonoobi, M.; Harun, J.; Mathew, A. P.; Oksman, K. Mechanical Properties of Cellulose Nanofiber (CNF) Reinforced Polylactic Acid (PLA) Prepared by Twin Screw Extrusion. *Compos. Sci. Technol.* **2010**, *70*, 1742−1747.
(31) Pei, A.; Malho, J.-M.; Ruokolainen, J.; Zhou, Q.; Berglund, L. A. Strong Nanocomposite Reinforcement Effects in Polyurethane Elastomer with Low Volume Fraction of Cellulose Nanocrystals. *Macromolecules* **2011**, *44*, 4422−4427.
(32) Mendez, J.; Annamalai, P. K.; Eichhorn, S. J.; Rusli, R.; Rowan, S. J.; Foster, E. J.; Weder, C. Bioinspired Mechanically Adaptive Polymer Nanocomposites with Water-Activated Shape-Memory Effect. *Macromolecules* **2011**, *44*, 6827−6835.
(33) Auad, M. L.; Richardson, T.; Hicks, M.; Mosiewicki, M. A.; Aranguren, M. I.; Marcovich, N. E. Shape Memory Segmented Polyurethanes: Dependence of Behavior on Nanocellulose Addition and Testing Conditions. *Polym. Int.* **2012**, *61*, 321−327.
(34) Agarwal, P.; Chopra, M.; Archer, L. A. Nanoparticle Netpoints for Shape-Memory Polymers. *Angew. Chem., Int. Ed.* **2011**, *50*, 8670−8673.
(35) Zhu, Y.; Hu, J. L.; Luo, H.; Young, R. J.; Deng, L. B.; Zhang, S.; Fan, Y.; Ye, G. D. Rapidly Switchable Water-Sensitive Shape-Memory Cellulose/Elastomer Nano-Composites. *Soft Matter* **2012**, *8*, 2509−2517.
(36) Zhou, S.; Deng, X.; Yang, H. Biodegradable Poly(ε-Caprolactone)-Poly(Ethylene Glycol) Block Copolymers: Characterization and Their Use as Drug Carriers for a Controlled Delivery System. *Biomaterials* **2003**, *24*, 3563−3570.
(37) Bondeson, D.; Mathew, A.; Oksman, K. Optimization of The Isolation of Nanocrystals from Microcrystalline Cellulose by Acid Hydrolysis. *Cellulose* **2006**, *13*, 171−180.
(38) Capadona, J. R.; Van Den Berg, O.; Capadona, L. A.; Schroeter, M.; Rowan, S. J.; Tyler, D. J.; Weder, C. A Versatile Approach for the Processing of Polymer Nanocomposites with Self-Assembled Nanofibre Templates. *Nat. Nanotechnol.* **2007**, *2*, 765−769.
(39) Yu, X. J.; Zhou, S. B.; Zheng, X. T.; Guo, T.; Xiao, Y.; Song, B. T. A Biodegradable Shape-Memory Nanocomposite with Excellent Magnetism Sensitivity. *Nanotechnology* **2009**, *20*, 235702.
(40) Liu, Y.; Li, Y.; Chen, H.; Yang, G.; Zheng, X.; Zhou, S. Water-Induced Shape-Memory Poly(D,L-Lactide)/Microcrystalline Cellulose Composites. *Carbohydr. Polym.* **2014**, *104*, 101−108.
(41) Shao, S.; Li, L.; Yang, G.; Li, J.; Luo, C.; Gong, T.; Zhou, S. Controlled Green Tea Polyphenols Release from Electrospun PCL/Mwcnts Composite Nanofibers. *Int. J. Pharm.* **2011**, *421*, 310−320.
(42) Marcovich, N.; Auad, M.; Bellesi, N.; Nutt, S.; Aranguren, M. Cellulose Micro/Nanocrystals Reinforced Polyurethane. *J. Mater. Res.* **2006**, *21*, 870−881.

DOI: 10.1021/am5081056
ACS Appl. Mater. Interfaces 2015, 7, 4118−4126

(43) Zhao, Q.; Sun, G.; Yan, K.; Zhou, A.; Chen, Y. Novel Bio-Antifelting Agent Based on Waterborne Polyurethane and Cellulose Nanocrystals. *Carbohydr. Polym.* **2013**, *91*, 169−174.
(44) Favier, V.; Canova, G.; Cavaillé, J.; Chanzy, H.; Dufresne, A.; Gauthier, C. Nanocomposite Materials from Latex and Cellulose Whiskers. *Polym. Adv. Technol.* **1995**, *6*, 351−355.
(45) Cao, X.; Habibi, Y.; Lucia, L. A. One-Pot Polymerization, Surface Grafting, and Processing of Waterborne Polyurethane-Cellulose Nanocrystal Nanocomposites. *J. Mater. Chem.* **2009**, *19*, 7137−7145.
(46) Gu, X.; Mather, P. T. Entanglement-Based Shape Memory Polyurethanes: Synthesis and Characterization. *Polymer* **2012**, *53*, 5924−5934.
(47) Hu, H.; Dorset, D. L. Crystal Structure of Poly(ε-Caprolactone). *Macromolecules* **1990**, *23*, 4604−4607.
(48) Takahashi, Y.; Tadokoro, H. Structural Studies of Polyethers, $(-(CH_2)_m-O-)_n$. X. Crystal Structure of Poly(Ethylene Oxide). *Macromolecules* **1973**, *6*, 672−675.
(49) Wu, Q.; Henriksson, M.; Liu, X.; Berglund, L. A. A High Strength Nanocomposite Based on Microcrystalline Cellulose and Polyurethane. *Biomacromolecules* **2007**, *8*, 3687−3692.
(50) Tsagaropoulos, G.; Eisenberg, A. Dynamic Mechanical Study of the Factors Affecting the Two Glass Transition Behavior of Filled Polymers. Similarities and Differences with Random Ionomers. *Macromolecules* **1995**, *28*, 6067−6077.
(51) Thapa, A.; Miller, D. C.; Webster, T. J.; Haberstroh, K. M. Nano-Structured Polymers Enhance Bladder Smooth Muscle Cell Function. *Biomaterials* **2003**, *24*, 2915−2926.
(52) Yang, B.; Huang, W.; Li, C.; Li, L. Effects of Moisture on The Thermomechanical Properties of a Polyurethane Shape Memory Polymer. *Polymer* **2006**, *47*, 1348−1356.
(53) Qi, X.; Yao, X.; Deng, S.; Zhou, T.; Fu, Q. Water-Induced Shape Memory Effect of Graphene Oxide Reinforced Polyvinyl Alcohol Nanocomposites. *J. Mater. Chem. A* **2014**, *2*, 2240−2249.
(54) Gu, X.; Mather, P. T. Water-Triggered Shape Memory of Multiblock Thermoplastic Polyurethanes (TPUs). *RSC Adv.* **2013**, *3*, 15783−15791.
(55) Behl, M.; Lendlein, A. Shape-Memory Polymers. *Mater. Today* **2007**, *10*, 20−28.
(56) Chae Jung, Y.; Hwa So, H.; Whan Cho, J. Water-Responsive Shape Memory Polyurethane Block Copolymer Modified with Polyhedral Oligomeric Silsesquioxane. *J. Macromol. Sci., Part B: Phys.* **2006**, *45*, 453−461.

DOI: 10.1021/am5081056
ACS Appl. Mater. Interfaces 2015, 7, 4118−4126